(1)

Laboratory validation of nonlinear shoaling computations

A. Sheremet and M. Stiassnie

CAMERI - Coastal and Marine Engineering Research Institute, Technion, Haifa 32000, Israel, Fax: 9724-8227661, Tel.: 9724-8220642,
Email: alex@cameri2.technion.ac.il, miky@cameri2.technion.ac.il

Abstract

We investigate the performance of a nonlinear mathematical model against shoaling waves flume measurements, from both the spectral and bispectral evolution points of view.

A JONSWAP spectrum with $\gamma = 2.8$, representative of waves measured in the eastern Mediterranean, was used to simulate the deep water spectral density.

The wave evolution was simulated numerically using the unidirectional nonlinear deterministic model, which accounts for wave shoaling and second order (quadratic) nonlinear interaction. The model describes the evolution of arbitrary wide spectra all the way from deep into shallow water, under the restriction of a mildly varying topography.

The results of the numerical simulations agree well with the measurements. The nonlinear model predictions based on the phases sets derived directly from the spectral analysis of measured data describe well the evolution of the spectrum, in spite of relatively high dispersion; the numerically simulated bispectra also agree well with the measurements. The simulations using uniformly distributed random phases (a more realistic frame of work in many applications) yield also good results for the power-spectrum evolution, but are less successful in describing the evolution of the bicoherence, for all the data batches that were simulate. Overall, the performance of the unidirectional model is good and highlights the usefullness of the numerical modelling for processes in the shoaling zone.

Introduction

As ocean waves propagate through water of decreasing depth, they undergo a spectacular and irreversible change: the shape of individual waves changes from almost symmetrical in deep water to one exhibiting sharp crests and broad, flat troughs in shallow water, where

they eventually break. Aside from the theoretical interest these processes arise, one cannot overstate the importance of the practical aspects. Features like strength, dimension and operability of coastal structures are decided upon on the basis of significant parameters of the wave field such as characteristic length, period and height, and the associated mean flow and water level. The energy transferred to the long waves is closely associated to the with surf beats and low frequency harbour oscillations that resonate moored ships. At open sea the long waves are nearly absent from the spectrum. They are generated through nonlinear interaction among wind waves mostly close to the shore, within a domain of a few tens of wave-lengths, a process associated to strong phase correlations.

The evolution of the shoaling ocean waves is essentially a nonlinear one: important transfers of energy take place among the spectral components, leading to the development of secondary peaks at superharmonics of the spectral peak frequency and the generation of subharmonics, often called long waves. The statistical nature of the surface evolves also from Gaussian to one characterized by nonzero odd-order correlators so that in a certain sense, the description of the wave field solely by means of the power spectrum is no longer adequate, and one has to look at higher order spectra.

This report presents some results of a study conducted to investigate the capabilities of the nonlinear unidirectional shoaling model developed by Agnon et.al.(1993). The model describes the evolution of arbitrary wide spectra all the way from deep into shallow water, taking into account the full form of the dispersion relation and the quadratic nonlinear interactions (among triads of waves).

The unidirectional shoaling model

The evolution equation

The equations governing the irrotational flow of an inviscid fluid with a free surface, after expanding the surface boundary conditions in power series about $z = 0$ and discarding all terms higher than quadratic, are:

$$
\begin{aligned}
&\nabla^2\phi + \phi_{zz} = 0 \qquad \text{in} \quad -h \le z \le 0,\\
&\phi_z + \nabla h \cdot \nabla\phi = 0 \qquad \text{on} \quad z = -h,\\
&\phi_{tt} + g\phi_z = \left[-\frac{1}{2}|\nabla\phi|^2 - \frac{1}{2}(\phi_z)^2 + \frac{1}{g}\phi_t\phi_{zt}\right]_t - \nabla\cdot(\phi_t\nabla\phi) \qquad \text{on} \quad z = 0,\\
&g\eta = -\phi_t + \frac{1}{g}\phi_t\phi_{zt} - \frac{1}{2}|\nabla\phi|^2 - \frac{1}{2}(\phi_z)^2 \qquad \text{on} \quad z = 0,
\end{aligned}
\tag{1}
$$

where ∇ is the horizontal gradient and ϕ, η and h are the velocity potential, the free surface displacement and the local water depth, respectively. The origin of the reference frame is taken in deep water at the still water level, with the z axis upwards. The first three equations form a closed system for ϕ, and η is given as a function of ϕ via the last equation in system (1).

We shall assume that most of the spectrum is in intermediate water depth in most of the domain under consideration, which is to say that $kh = O(1)$, with k the characteristic wave number. Also, that the beach slope is mild, that is $|\nabla h| = O(\epsilon)$. The small paremeter ϵ is the order of magnitude of the characteristic wave steepness ka, with a the characteristic amplitude of the waves.

The main task in the derivation of the evolution equation for a shoaling directional gravity-wave spectrum is to reduce the three-dimensional system (1) to a single equation by eliminating the vertical structure of the function ϕ. For the details of the original derivation of the unidirectional shoaling model, the reader is directed to the article by Agnon et.al.(1993); a more general result, for three-dimensional geometries, was given by Sheremet(1996). Here we shall confine ourselves only to describe the final results of their works.

For the case of a unidirectional wave field propagating normally towards the shore, the resulting equation for the complex amplitude of ϕ reads:

$$\frac{\partial A}{\partial t}+\frac{1}{2}A\frac{\partial C_g}{\partial x}+C_g\frac{\partial A}{\partial x}=\int_{-\infty}^{\infty}\mathrm{W}_{0:1,2}A_1A_2e^{-i\int_{-\infty}^{x}(k-k_1-k_2)dx}\delta^{\omega}_{0:1,2}d\omega_{1,2}$$

$$\mathrm{W}_{0:1,2}=\frac{1}{8\pi}\left[2k_1k_2+(\sigma_1\sigma_2)^2+k_1^2\frac{\sigma_2}{\sigma}+k_2^2\frac{\sigma_1}{\sigma}-\sigma^2\sigma_1\sigma_2\right]. \tag{2}$$

where the amplitude A is defined by:

$$\phi=A\frac{\cosh[k(z+h)]}{\cosh(kh)}e^{-i\int kdx},$$

$$\sigma_j^2=\frac{\omega_j^2}{g}=k_j\tanh(k_jh) \tag{3}$$

and $C_g=\frac{\partial\omega}{\partial k}$ is the group velocity.

For numerical integrations purposes the above equation may be brought to a discrete form, by writing for the velocity potential the Fourier expansion:

$$\phi=-\frac{i}{2}\sum_{j=1}^{\infty}\left[A_je^{i(\int k_jdx-\omega_jt)}-A_j^*e^{-i(\int k_jdx-\omega_jt)}\right], \tag{4}$$

with $\omega_j=j\omega$, $j\in\mathbf{N}$. Substitution of the above into (2) gives the discrete equation:

$$\frac{\partial A_j}{\partial t}+\frac{1}{2}A_j\frac{\partial C_{g,j}}{\partial x}+C_{g,j}\frac{\partial A_j}{\partial x}=$$

$$\sum_{\alpha=1}^{\infty}\sum_{\beta=1}^{\infty}\mathrm{V}^{(1)}_{j,\alpha,\beta}A_\alpha A_\beta e^{-i\int_{-\infty}^{x}(k_j-k_\alpha-k_\beta)dx}\delta^{\omega}_{j:\alpha,\beta}d\omega_{\alpha,\beta}-$$

$$-\sum_{\alpha=1}^{\infty}\sum_{\beta=1}^{\infty}2\mathrm{V}^{(2)}_{j,\alpha,\beta}A_\alpha^*A_\beta e^{-i\int_{-\infty}^{x}(k_j+k_\alpha-k_\beta)dx}\delta^{\omega}_{\beta:j,\alpha}d\omega_{\alpha,\beta} \tag{5}$$

The discrete kernels in Equation 5 are:

$$\mathrm{V}^{(1)}_{j,\alpha,\beta}=\frac{1}{8}\left[2k_\alpha k_\beta+(\sigma_\alpha\sigma_\beta)^2+k_\alpha^2\frac{\sigma_\beta}{\sigma}+k_\beta^2\frac{\sigma_\alpha}{\sigma_j}-\sigma_j^2\sigma_\alpha\sigma_\beta\right],$$

$$\mathrm{V}^{(2)}_{j,\alpha,\beta}=\frac{1}{8}\left[-2k_\alpha k_\beta+(\sigma_\alpha\sigma_\beta)^2+k_\alpha^2\frac{\sigma_\beta}{\sigma}-k_\beta^2\frac{\sigma_\alpha}{\sigma_j}+\sigma_j^2\sigma_\alpha\sigma_\beta\right]. \tag{6}$$

Equation (5) is the unidirectional shoaling model whose performance will be tested in the sequel against laboratory measurements. Given appropriate initial conditions, Equation (5) may be integrated numerically to yield the spectral amplitudes A_j at any location inside the shoaling domain. Several problems related to the initial conditions are discussed in the next subsection.

The initial conditions

If the Fourier modes are known at a certain location, Equation (5) may be integrated numerically to obtain the wave power spectrum evolution along the whole shoaling region. The model requires the full spectral information about the sea state at the starting point (say, at deep water), that is, both information about the spectral density and about the modal phases. Quite often, the former is available, but phase information is less common. For example, the spectral data provided by a stochastic third-generation deep-sea wave forecasting model, that would commonly be used to provide initial conditions, contains no phase information.

When the initial spectrum is known but the phase information is absent, the model may still be integrated under the assumption that the sea is Gaussian at the starting point (the initial phases are uniformly distributed). This is another way of saying that at the starting point (deep water, usually), there is no significant information in the modal phases, and a realization of the sea may be obtained by simply generating a set of uniformly distributed random phases to attach to the known modal amplitudes. An unlimited number of realizations of the sea surface may be obtained this way; the statistical picture of the waves evolution is obtained by averaging the results of several runs of the model.

The answer to the question as to how many realizations one should shoal to obtain a realistic picture of the spectral evolution is ultimately decided by hardware limitations. The experience has shown that a number between 50 and 100 runs yields a rather stable estimation of the spectral evolution, which is fortunate if one takes into account that even with this relatively small number of sets, a 50 realizations run of a 60 spectral components spectrum takes more than two days to complete (on an Digital AlphaStation250$^{4/266}$ using $\sim$ 100 % of processors resources).

Measurements: data assimilation and reduction

The Bathymetry

The measurements were performed in the CAMERI[1] towing tank, which is 48m long, 2.45m wide and 1.5m deep, using a model (scale 1:40) of the bathymetry in front of of the Acre Harbour. Wave reflection was prevented by a sloped beach at the end of the tank opposite to the wave-maker. The part of the beach that was of interest for the present simulations starts at 30m depth (prototype). The evolution of the waves was monitored from 30m depth to the 6m depth (prototype), at 13 locations uniformly distributed along a region roughly divided into two segments; the first having a slope of about 5%, from 30 to 8m depth, and the second with a slope of about 1%, from 8 to 6m depth (see Figure 1). Most of the nonlinear evolution occured within the second shorter and shallower segment.

Waves simulation

The sea waves were simulated by generating irregular waves by means of a wavemaker located at the prototype depth of 30m, 5m in front of the first wave gauge. A JONSWAP spectrum with $\gamma = 2.8$, representative of waves measured in the eastern Mediterranean,

[1]CAMERI - Coastal and Marine Engineering Research Institute, Technion, Haifa 32000, Israel

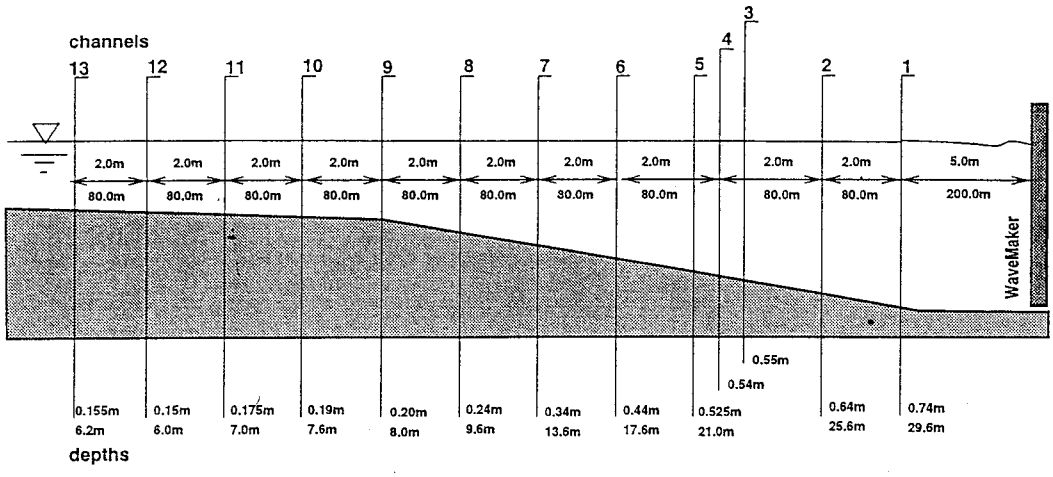

Figure 1: Bathymetry and wave gauges locations. The geometrical scale is 1:40. The vertical lines mark the locations of the wave gauges.

was used to simulate the deep water spectral density. The duration of each simulation was 20 minutes, at a sampling frequency of 25Hz. At the prototype scale this is equivalent to a duration of about1 hour and 25 minutes, at a sampling rate of about 4Hz . The data used in the simulations, consisting of 10 storms, is given in the table below:

Peak periods (s)	9.4	10.9	12.2	13.4	14.4
Significant Heights (m)	2.3	2.0	2.2	1.6	1.9
Significant Heights (m)	2.0	1.6	1.5	1.3	1.4

and comprises two groups of runs with different significant heights for each of the peak periods. In the first group of runs, (the higher waves batch), occasional breaking in the form of plunging and spilling breakers was observed within the most shallow section of the domain. During the second batch (lower waves), the water was much quieter, with no plunging breakers observed. A relative decay of about 15% in the linear estimation of the total energy flux occuring at the shallow end of the flume seems to indicate that breaking might have occurred in the form of spilling, at this scale usually as cappillary waves generated at the peak of the wave.

The Spectra

The water level was measured simultaneously at 13 locations uniformly distributed along the frontal part of the beach, from the depth of 30m to a depth of 6.2m (see Figure 1), by means of resistance type gauges.

Since the aim was to test a numerical model against the results of the experiment, the processing capabilities of the computer had to be taken into account, in that we had to strike a balance between the precision of data reduction and the speed of the numerical processing. As mentioned before, a 50 realizations run of a 60 spectral components spectrum seemed to be a reasonable target. With these criteria in mind, standard spectral analysis was applied to each of the 13 channels: the time series were broken up into overlapping sequences of 1024 data points each; the result was 50 sequences each one of about 20 waves for the run with the longest peak period in the group (14.4s), and about

30 waves for the run with the shortest ($T_p = 9.0s$) wave. The sequence length of 1024 points was chosen to provide a better numerical description of the spectral density with fewer Fourier modes - for the numerical integrations only the longest 60 spectral components were used. Each individual sequence was windowed using a Hanning window, then transformed to the frequency domain usin standard FFT routines. The sample spectral densities were then averaged to obtain the power spectra.

We shall not present results for all cases analyzed, since they exhibit similar trends, but instead will try to limit the discussion to the representative features of the data. Figure 2 illustrates the evolution of the measured spectral density for the higher wave of the two runs with peak period T=12.2s, at stations No. 1, 9,11,12. The nonlinear energy transfer from the peak of the spectrum to its first and second harmonic is striking, so is the excitation of the longer waves in the spectrum. Three frequency domains are separated by vertical lines: a 'long wave' with the upper boundary at about 25s, a 'medium waves' domain between ~25s and ~9s and a 'short waves' one for waves with a period less than ~9s. It should be stressed that this division is done here only to separate the peak from its harmonics. For each domain we define a 'significant height' by the relation

$$H_{\text{domain}} = 4\sqrt{\sum_{f_1}^{f_2} S(f)df} \tag{7}$$

where 'domain' stands for 'long', 'medium' or 'short' and f_1 and f_2 are the corresponding frequency limits. The above parameter may be regarded as a convenient and intuitive way to describe the energy within a certain frequency interval. The evolution of the partial 'significant heights' is plotted in Figure 3.

The data obtained from measurements at the first station, the one closest to the wave maker, was used in the initialization of the numerical model. For runs under the assumption of a Gaussian sea, the power spectrum at the first station was completed with different sets of randomly distributed initial phases generated on the computer and fed to the model as initial conditions. The results of the numerical integrations were then averaged to obtain the final evolution of the spectrum.

For the case of true phases sets, the data processing was somewhat different. After breaking the time series into sequences, the individual sequences were transformed to the frequency domain straight away, without windowing; the resulting complex Fourier sequences were truncated to 60 components, which were used as initial conditions. The spectral estimates at the locations along the shoaling region were obtained by first windowing and then averaging the results of the numerical integrations.

The bicoherence

Since the work of Hasselman et.al.(1963), higher order spectral analysis has achieved a undisputed status as a tool in the study of non-Gaussian nonlinear processes (for a sistematic application to nonlinear waves in shallow water see for example Elgar and Guza, 1986 and the references therein). Following are the definitions of bispectra and bicoherence as used in this work.

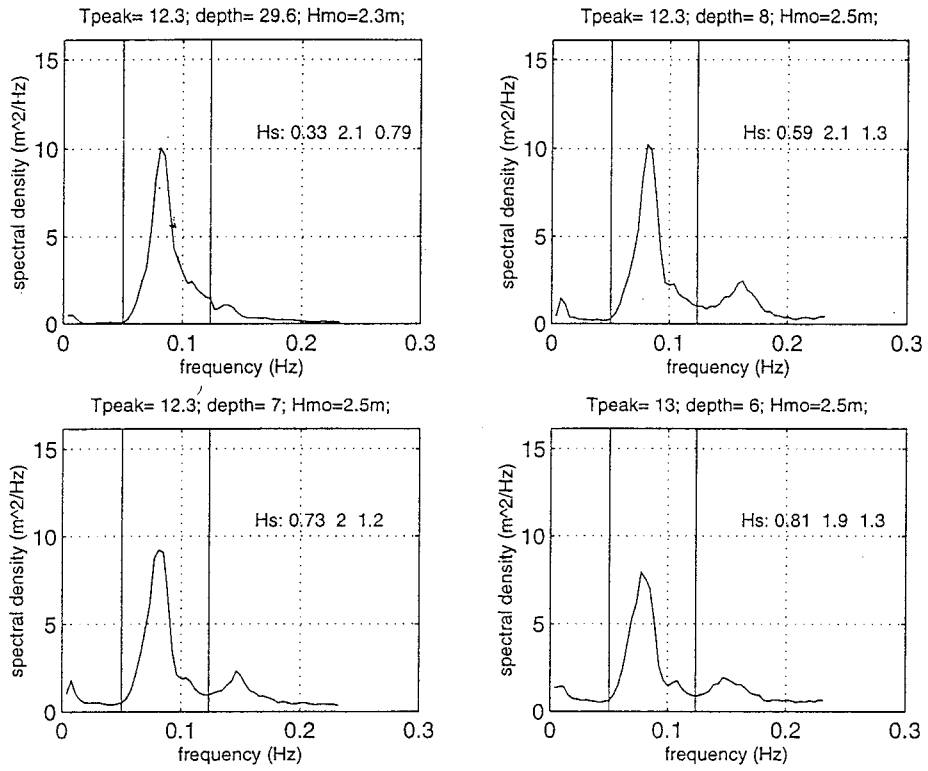

Figure 2: The evolution of the measured spectral density at four locations, stations 1 (30m), 9 (8m), 11 (7m) and 12 (6m), for wave $T_p = 12.2s, H_s = 2.1m$. Inset shows the partial 'significant heights' for the long, medium and short waves, in this order.

Let a real stationary random process be represented as a truncated Fourier series

$$\xi(x,t) = \sum_{n=1}^{N} \left[A_n e^{i(k_n x - \omega_n t)} + A_n^* e^{-i(k_n x - \omega_n t)} \right] \tag{8}$$

with k the wave-number given by the linear dispersion relation, ω the radial frequency and A a complex coefficient. The bispectrum is defined as the Fourier transform of the third order cumulant:

$$\begin{aligned} \mathcal{B}(\omega_1, \omega_2) &= \left(\frac{1}{2\pi}\right)^2 \int_{-\infty}^{\infty} \mathcal{C}(\tau_1, \tau_2) e^{-i\omega_1\tau_1 - i\omega_2\tau_2} d\tau_1 d\tau_2 \\ \mathcal{C}(\tau_1, \tau_2) &= \langle \xi(t)\xi(t+\tau_1)\xi(t+\tau_2) \rangle \end{aligned} \tag{9}$$

where $\mathcal{C}$ is the third order cumulant and the triangular brackets stand for the averaging operator. For discretely sampled data the digital bispectrum is given by:

$$\mathcal{B}(\omega_k, \omega_j) = \langle A_{\omega_k} A_{\omega_j} A^*_{\omega_k + \omega_j} \rangle \tag{10}$$

The bispectrum as defined in (10) will most probably exhibit higher values for higher values of the $\langle |A_{\omega_k}|^2 \rangle$, as higher means yield usually higher variances. For this reason, in order to isolate the phase correlations alone, it is convenient to normalize the bispectrum. Different combinations have been tried in literature; in this work the normalized

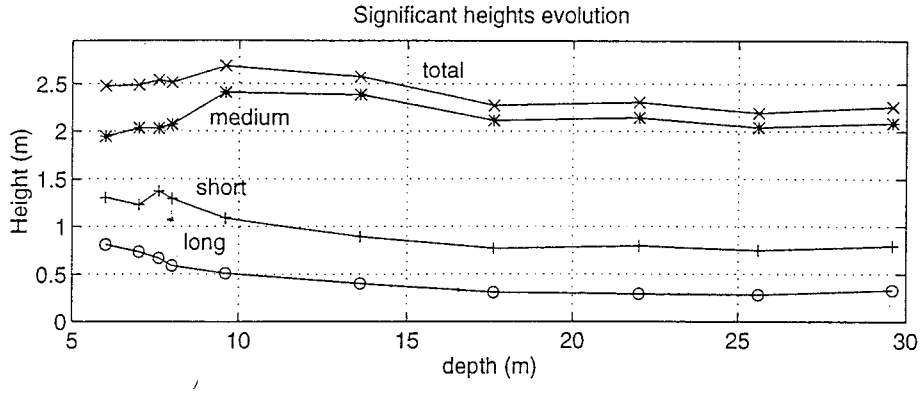

Figure 3: The evolution of the measured total and the partial 'significant heights' for the long, medium and short waves, for the wave with $T_p = 12.2s$, $H_s = 2.1m$.

magnitude of the bispectrum, called the bicoherence, is defined, as in Kim and Powers (1979):

$$b^2(\omega_k, \omega_j) = \frac{|\mathcal{B}(\omega_1, \omega_2)|^2}{\langle |A_{\omega_k} A_{\omega_j}|^2 \rangle \langle |A_{\omega_k + \omega_j}|^2 \rangle} \tag{11}$$

which yields a value between 0 and 1. For a Gaussian field the bicoherence is close to zero. If there are phase correlations between the modes k and j, the bicoherence will exhibit a pronounced peak at the frequencies (ω_k, ω_j).

Figure 4 presents the measured time series bicoherence at four stations, 1^{st}, at depth 30m prototype, 6^{th} at 17.6m, 9^{th} at 8m depths and 11^{th} at 6m depth. As it may easily be seen from the definition, the bicoherence function $b^2(\omega_k, \omega_j)$ is symmetrical with respect to the first diagonal, as the plots also show quite clearly. It is also easily shown that for the truncated Fourier spectra produced by the numerical model the region above the line $y = (1 - x) f_{max}$ has no meaning. For comparison between the numerical and experimental results, the reader should therefore confine his attention to what is drawn inside the white triangle alone. While in deep water, at the first station (30m prototype)the bicoherence is under the 0.3 level (taken here as the noise level), strong peaks start to develop towards the depths of 8m and remain strong throughout the shallower portion of the flume. As said before, a peak at coordinates (f_1, f_2) indicates a strong phase coupling between the spectral components of frequencies f_1, f_2 and $f_1 + f_2$. As expected, the peaks are located at harmonics of the absolute peak of the spectrum. It is interesting to notice that the phase correlations weaken slightly in the region where occasional breaking was observed. The first, deeper segment of the flume (up to station 9) does not seem to be very active in the generation of phase correlations either.

Numerical results

To illustrate the behaviour of the numerical model we shall present the numerical results of the integrations for the run with peak period $T_p = 12.2s$, significant height $H_s = 2.2m$.

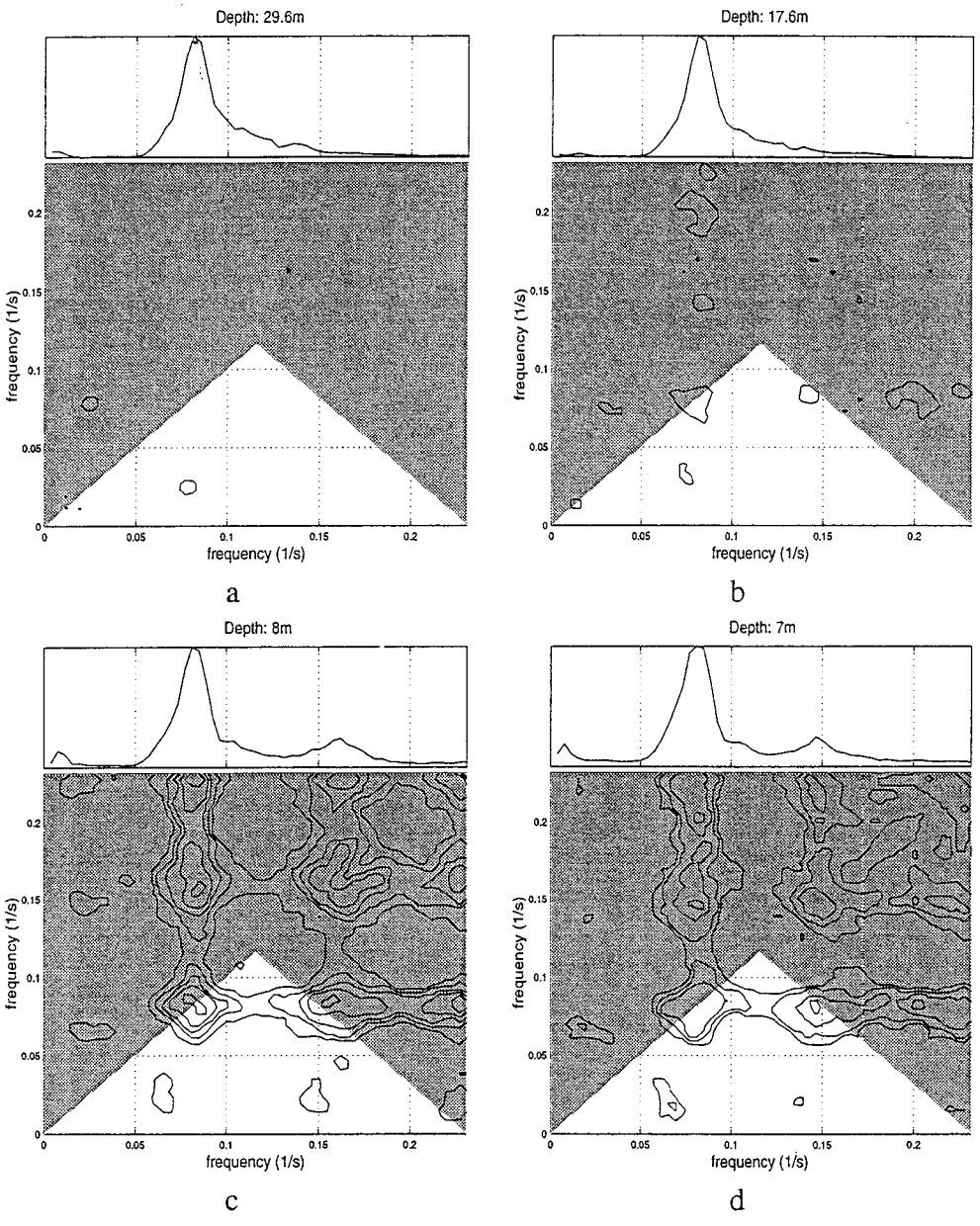

Figure 4: Smoothed bicoherence and normalized spectrum for the measured time series at four stations: a) 30m, b)17.6m, c) 8m and d) 6m, stations 1^{st}, 6^{th}, 9^{th} and 11^{th}respectively, for the wave with $T_p = 12.2s$ and $H_s = 2.1m$. The increment between the contour lines is 0.1; the lowest contour is 0.3.

The Spectra

Figure 5 shows the evolution of the spectral density for the runs with Gaussian initial conditions (measured initial spectra and uniformly distributed, computer generated random phases). The graphs corresponding to the numerical calculations are drawn in continuous lines. For comparison, the measured spectra points are plotted as circles. Inset are given, as in the previous graphs, the partial 'significant heights' for both the measurements and the simulations. The shaded area around the numerical spectra has a vertical span equal to the standard deviation. The 'significant heights' evolution is also given and compared to the measurements, together with the linear estimate of the total energy flux evolution.

Figure 6 show the evolution of the spectral density for the runs with correct initial conditions (measured initial spectra together with the corresponding measured initial set of phases). It is interesting to remark that contrary to our expectations, the true phases runs behave somewhat poorer than the random phases runs. Indeed, not only the agreement between the measured and the compuuted spectra is less good, the individual realizations have also a larger statistical dispersion, as shown by the span of the standard deviation.

The computed bicoherence for the wave ($T_p = 12.2s, H_s = 2.2m$) is presented in Figure 7 for the runs with uniformly distributed initial phases, and the runs with measured phases. As opposed to the spectral evolution, for the case of the bicoherence the integrations that started with correct initial phases develop stronger phase correlation than the ones with Gaussian initial conditions. Figure 7b exhibits the peaks marking all the phase correlations one would expect to see; two strong peaks, one corresponding to the phase coupling of the spectral peak with its second harmonic and another one for the peak-second-third harmonics phase coupling; three other smaller ones (at the bottom of the plot) that indicate the correlation between the long waves and the spectral peak and its harmonics. In Figure 7a the peaks involving the longer waves are lost in the surrounding noise, and the two stronger peaks appear much less proeminent.

Conclusions

We have studied the performance of a nonlinear mathematical model compared to a series of shoaling waves flume measurements, and analyzed its results using both the traditional second order spectral approach as well as the higher order spectral analysis. The wave evolution was simulated numerically using the unidirectional nonlinear deterministic model, which accounts for wave shoaling and second order (quadratic) nonlinear interaction. For the present mathematical model, the third order spectral analysis tools (bispectrum, bicoherence) are particularily useful since the mechanism for the energy transfer within the wave spectrum is in this case only intreractions among triads of waves.

The experiments were designed to reproduce typical severe sea conditions in the Mediterranean. For reasons of space we presented only one set of comparisons, for the wave with a peak period of 12.2 s and a significant height of 2.1m, which is representative of study as a whole.

The results of the numerical simulations of the spectral evolution of the waves are remarkably good, especially if one takes into account that the Acre batyhmetry is not the ideal testing ground for the present model: 5% slope means a jump of 20m in depth over a 400m long stretch, barely twice the deep water spectral peak wave-length, whereas the

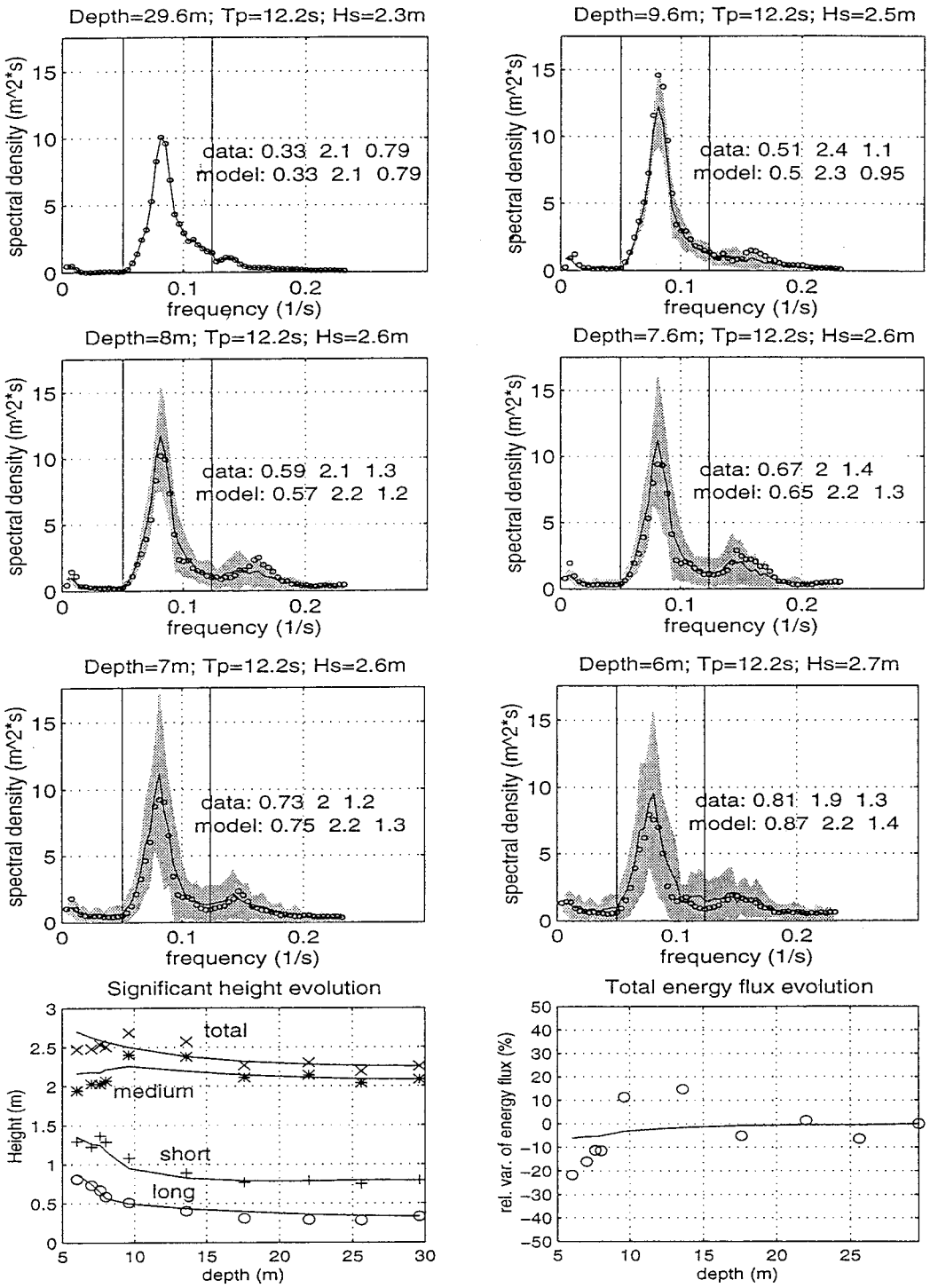

Figure 5: Spectral density, numerical model with uniformly distributed random initial phases, (line) compared to measurements (circles). Peak period $T_p = 12.2s$, initial significant wave height $H_s = 2.2m$. Inset: long, wind and short wave band significant wave heights, as given by the model and the measurements.Comparison of the evolution of the band significant wave heights (lower corner left, numerical simulations: lines) and total energy flux (lower corner, right).

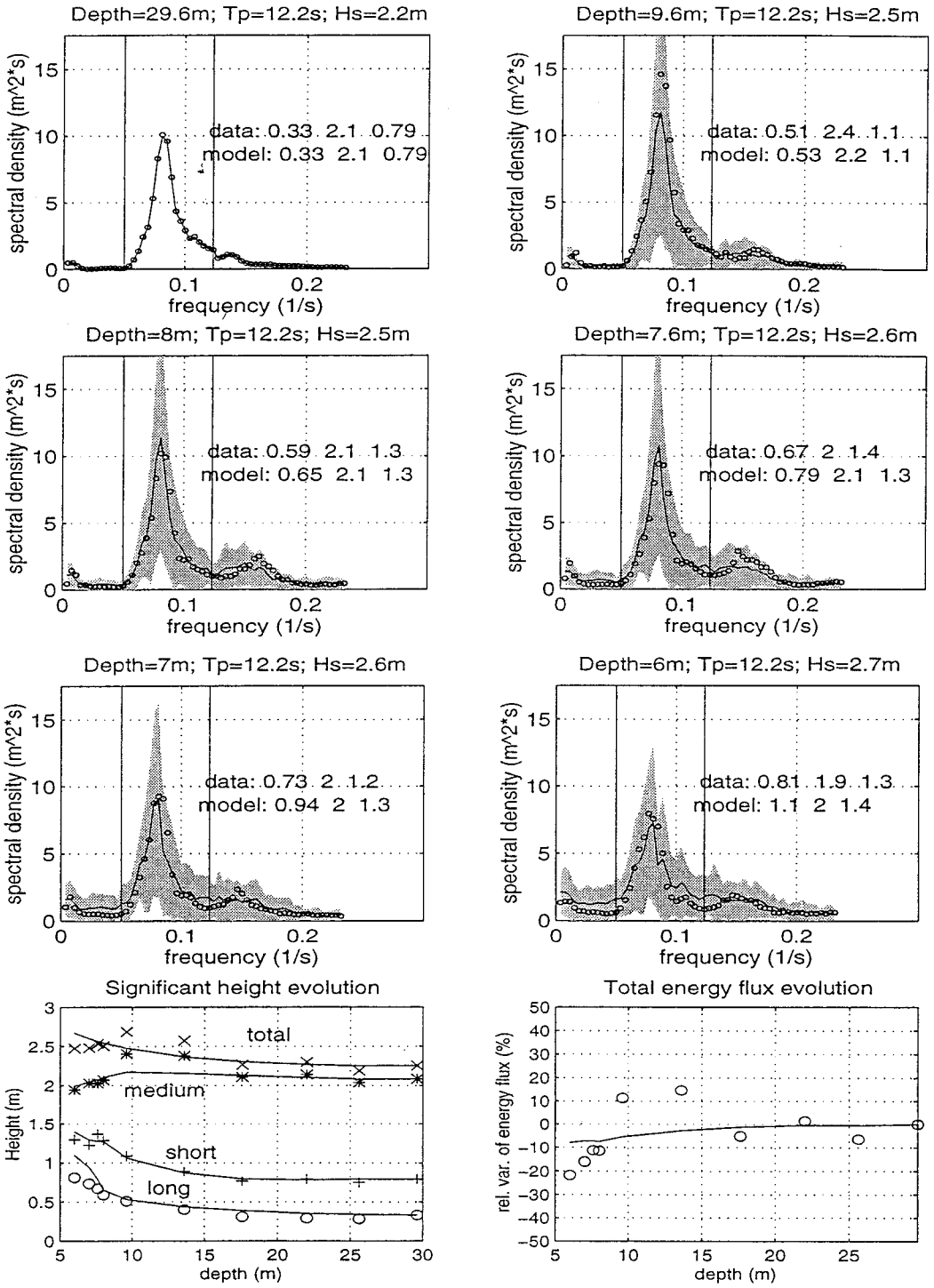

Figure 6: Spectral density, numerical model with measured initial phases, (line) compared to measurements (circles). Peak period $T_p = 12.2s$, initial significant wave height $H_s = 2.2m$. Inset: long, wind and short wave band significant wave heights, as given by the model and the measurements.Comparison of the evolution of the band significant wave heights (lower corner left, numerical simulations: lines) and total energy flux (lower corner, right).

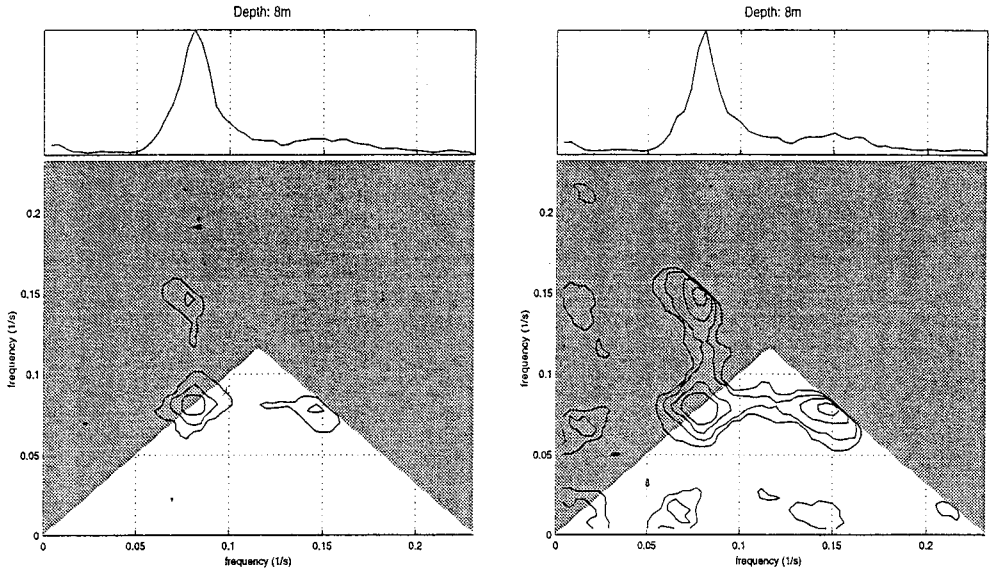

a b

Figure 7: Smoothed bicoherence and normalized spectrum for the computed time series at station 9, 8m depth for the wave with T_p=12.2s, H_s=2.2m. a) uniformly distributed initial phases. b) correct phases. The increment between the contour lines is 0.1; the lowest contour is 0.3.

model was developed under the specific restriction of a mild bottom slope (say 1%). Some interesting results regarding the capability of the numerical model to simulate the evolution of the phase correlations seem to indicate (not surprisingly) that the more Fourier components in the simulations, the better is the accuracy of the results. Since, however, the numerical effort increases faster than the square of the number of components in the spectrum, for the moment the limiting number is still rather low.

Overall, the results of the present work, indicate the usefullness of numerical models in the prediction of the wave evolution in the shoaling region.

Acknowledgements

Part of this research was supported by the fund for the promotion of research at the Technion.

References

Agnon, Y., Sheremet A., Gonsalves J. and Stiassnie M.(1993) *A unidirectional model for shoaling gravity waves*, Coastal Engineering, **20**, pp.29-58

Elgar S. and Guza R.T.(1986) *Nonlinear model predictions of bispectra of shoaling of gravity waves*, J.Fluid Mech. **167**, pp.1-18

Hasselmann K., Munk W. and MacDonald G. (1963) *Bispectra of ocean waves*, in Time Series Analysis, ed. M. Rosenblatt, pp.125-139

Kim Y.C. and Powers E.J. (1979) *Digital bispectral analysis and its application to nonlinear waves*, IEEE, Trans. Plasma. Sci.,**7** pp.120-131

Sheremet A. (1996) *Wave inteaction in shallow water*, Ph.D. Thesis, Technion-Israel Institute of Technology, Haifa, Israel.